A Mathematical Model of the Spray Deposition Process

E. GUTIERREZ-MIRAVETE, E.J. LAVERNIA,
G.M. TRAPAGA, J. SZEKELY, and N.J. GRANT

Spray deposition is a recently developed atomization process designed to produce high density, bulk metal shapes directly from the melt. The process consists of two basic steps: first, a molten metal stream is atomized using a gas; the spray thus produced is then collected onto a suitably designed substrate. In this paper a mathematical model for the analysis of heat transfer during SD is described. The model is in two parts: the first part calculates the thermal histories of atomized droplets in flight, whereas the second part computes the transient temperature profiles inside the growing preform. More specifically, the mathematical model estimates droplet size distribution, temperatures, fractional solidification and microstructures of the atomized droplets in the spray, and the temperature field and microstructure of the resulting deposit. In contrast with established views, the computed cooling rates during solidification in the preform are relatively low (1 to 10 °C/second). The results also indicate that a small fraction of liquid mixed with solid exists at the top of the growing preform during deposition. The tiny pools of liquid may play a role in the formation of the characteristic equiaxed grain microstructure of as-deposited preforms. The results of the calculations are very sensitive to the value of the enthalpy of the impinging spray. Therefore, the production of good quality deposits requires accurate control of the heat fluxes during deposition.

I. INTRODUCTION

ALTHOUGH numerous property improvements have been demonstrated to result from rapid solidification, commercialization has been limited, due to the difficulty involved in the production of bulk shapes and also to the oxide formation almost always associated with the particulate nature of the products of processing.[1–11,19,42] However, the recently developed spray deposition techniques, such as Osprey and the liquid dynamic compaction process, appear capable of producing dense, fine-grained, bulk specimens directly from the melt and with a minimum of oxidation.[12–22] Significant property improvements have been demonstrated to result from these processes in several alloy systems.[16–22]

The spray deposition process consists of two steps: first, a molten metal stream is fragmented by means of high speed gas jets; the resulting droplet dispersion is then collected onto a suitably designed substrate,[23,24,26] which may or may not be cooled, but generally is. Figure 1 is a schematic representation of a typical spray deposition process. Figure 16 shows the SD set-up at the University of California, Irvine. The spray formed during the atomization stage is rapidly quenched by the moving gas, so that the thermal conditions of the spray at the moment of impact with the deposit are determined by the amount of energy extracted from the drops by the gas. It should be noted that the thermal history of the preform is the result of the combined effects of the enthalpy content of the impinging spray, the heat loss from the top surface, and the rate of heat extraction by the underlying substrate. Since the structure and properties of the deposit are related to the thermal conditions during solidification, it is of interest to have some means of estimating heat transfer rates during spray deposition. The objective of this work is to obtain a better quantitative understanding of the process while using only a minimum of mathematics.

In the sequel, the formulation of the mathematical model of the spray deposition process is presented first, followed by a discussion of the main simplifying assumptions used in the model. The second half of the paper includes a discussion of results and a list of conclusions.

E. GUTIERREZ-MIRAVETE, Curriculum Chair and Assistant Professor, Department of Metallurgy, The Hartford Graduate Center, 275 Windsor Street, Hartford, CT 06120; also Research Affiliate, Department of Materials Science and Engineering, Massachusetts Institute of Technology, Cambridge, MA 02139. E.J. LAVERNIA is Assistant Professor, Department of Mechanical Engineering, University of California at Irvine, Irvine, CA 92717; formerly, Research Associate, Department of Materials Science and Engineering, Massachusetts Institute of Technology, Cambridge, MA 02139. G.M. TRAPAGA, Graduate Student, J. SZEKELY, Professor of Materials Engineering, and N.J. GRANT, Professor of Metallurgy, are at Department of Materials Science and Engineering, Massachusetts Institute of Technology, Cambridge, MA 02139.

Manuscript submitted April 8, 1987.

II. FORMULATION

Since spray deposition is a two-step process (*i.e.*, atomization and spray collection or deposition), it is useful to construct the model also as a two-part numerical algorithm. The first part is dedicated to the computation of the thermal histories of the atomized droplets in flight, whereas the second part computes the temperature distribution in the resulting preform during deposition. The mathematical formulation of these two parts of the model is presented in this section. Additional details can be found in References 72 and 73.

A. *The Atomization Step*

In order to compute the temperatures of the droplets in the spray one must calculate first their sizes and velocities. It is well known that the results of liquid metal atomization experiments often obey a correlation first given by Lubanska[25] and then modified by others.[26]

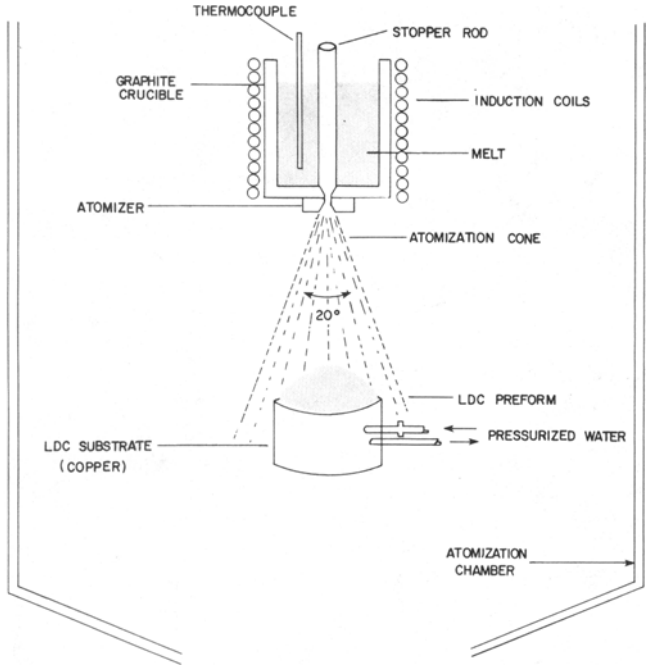

Fig. 1—Schematic representation of the spray deposition process.

According to this, the so-called mass mean droplet diameter (*i.e.*, the opening of a screening mesh which lets through 50 pct of the mass of the powder resulting from an atomization experiment performed in the absence of a collecting substrate), d_{50} is given by

$$d_{50} = K_d \left[\frac{\eta_m d_0 \sigma_m}{\eta_g v_g^2 \sigma_m} \left(1 + \frac{J_{\text{melt}}}{J_{\text{gas}}} \right) \right]^{1/2} \quad [1]$$

where

$$J_{\text{melt}} = 2 A_o \rho_m C_D (2 g h_c)^{1/2} \quad [2]$$

and

$$J_{\text{gas}} = A_t \left[\gamma \rho_g p_o \left\{ \frac{2}{\gamma + 1} \right\}^{\left(\gamma + 1/\gamma - 1 \right)} \right]^{1/2} \quad [3]$$

and

$$\rho_g = 2.7(1.6317 * 10^{-5} p_o + 1.0585) \quad [4]$$

The meanings of all the terms in these equations are collected in the Nomenclature at the end of the paper.

Some comments are in order regarding Eqs. [1] through [4]. First, an empirical factor of two has been included in Eq. [2] to account for the frequently observed "aspiration" of metal from the crucible by the atomizing gas.[28] Equation [3] is rigorously valid for quasi-one-dimensional flows in choked nozzles,[63] while the flow in typical atomization nozzles is tridimensional, turbulent, and much more complicated. Ultimately, the calculation of gas flows in commonly used atomization nozzles must be done using numerical techniques.[64] Equation [3] is used here because it gives an estimate of the prevailing gas flow rate, and there does not seem to exist any other alternatives of comparable simplicity. Also, an effective throat area of nozzle A_t has been used. Although A_t is somewhat different from the actual throat area, it leads to good agreement between calculated and measured values of the gas velocity at the exit of the nozzle.[29,52] The exit gas velocities used in our calculations correspond to a Mach of 1.9, which is well within the range of the values recently measured and reported in Reference 52. Finally, Eq. [4] is simply an empirical correlation to account for the effect of the plenum pressure and the expansion cooling on the gas density.

By introducing appropriate values as given in Table I, Eqs. [1] through [4] give $d_{50} = 80$ microns. Moreover, from the statistical properties of the drop size, distribution one also obtains $d_{16} = 23$ microns and $d_{84} = 275$ microns. The values 23 microns and 275 microns are considered as characteristic of, respectively, the smallest and largest droplet sizes present in the atomized spray. These values of atomized particle size are within the range encountered in the laboratory when no collecting substrate is used and the droplets solidify in flight.[31] Therefore, we assume that Eqs. [1] through [4] provide a means of estimating the droplet size distribution obtained during gas atomization of liquid metals.

Once the droplet size distribution has been determined (either by using Eqs. [1] through [4] or by any other means, *e.g.*, empirically), the droplet velocities can be calculated from a simple force balance on a given drop of volume V_d[32];

$$\rho_d V_d \frac{dv_d}{dt} = V_d(\rho_d - \rho_g) g + (A_d/8) C_{\text{drag}} \rho_g (v_g - v_d) |(v_g - v_d)| \quad [5]$$

Table I. Input Data (Units as Given in Nomenclature)

Quantity	Value
a	45
A_s	0.0153
A_t	0.0000056
b	0.25
C_D	0.959
C_p (gas)	518.8
C_p (melt)	862.5
d_o	0.0026
H_f	397,746.0
H	198,873.0
h_{bot}	500.0
h_{top}	21.0
k (gas)	0.01636
k (melt)	209.2
K	2.0
K_d	162
p_o	$2.5 * 10^6$
Q_m	0.0308
T_o	0.0
T_L	740.0
T_S	660.0
T_{sub}	25.0
γ	1.65
ΔT_s	50 to 300
ΔT_u	20 to 40
σ_m	0.840
ρ_g	1.654
ρ_m	2700.0
μ_g	$1.7 * 10^{-5}$
μ_m	0.001

The two terms on the right-hand side of Eq. [5] represent, respectively, the gravitational force acting on the droplet and the accelerating force exerted on the droplet by the atomizing gas. Furthermore, the instantaneous position of the droplet along the atomization chamber can be readily obtained by solving

$$v_d = \frac{dz}{dt} \qquad [6]$$

As expected, only a fair agreement has been obtained when using Eqs. [5] and [6] for the calculation of droplet trajectories in other atomization systems of engineering interest (*e.g.*, combustion of liquid fuels[65]). Despite this, Eq. [5] provides a quick estimate of droplet velocities which is of the correct order of magnitude. More work is required in this case also in order to verify the appropriateness of this expression.

The value of C_{drag} can be obtained from Reference 33

$$C_{\text{drag}} = 0.28 + 6/N_{\text{Re}}^{0.5} + 21/N_{\text{Re}} \qquad [7]$$

as suggested in Reference 44 and despite the fact that the value of N_{Re} in Spray Deposition is equal to or greater than the upper limit of validity for this correlation. Finally, the gas velocity, v_g, is assumed to be a quadratic function of the flight distance,[47] although other functions can be readily incorporated. Indeed, recent experimental work[52] indicates that the rate of decay of the gas velocity with distance from the atomization point is faster than that calculated from a quadratic relationship. Since we did not have available the information in Reference 52 when these calculations were carried out, the results presented below assume a quadratic dependency of the gas velocity on the vertical distance. Summing up, although it is not expected that Eq. [5] can provide accurate values of droplet velocities, it should give results of the correct order of magnitude, and this is all we are aiming for in this first effort at tackling the problem.

The microstructure of the final deposit in a limited way, is, related to the state of the droplets impinging on the top surface of the growing preform. Therefore, in order to characterize the state of the droplets at the time of impingement on the preform, a thermal balance on the flying droplets must be carried out. The atomized droplets lose heat mostly by convection to the surrounding gas. For any given droplet, there are several possible states at the time of impingement, depending mostly on its size and on the presence of internal crystallization nuclei. Some possible states are:

(a) fully solid droplet (particle);
(b) fully liquid droplet with a temperature above the liquidus;
(c) partially solidified droplet with a temperature between the liquidus and solidus;
(d) fully liquid droplet with a temperature below the liquidus (undercooled droplet).

Since the spray contains particles with sizes in the range between, say 20 and 300 microns, one can expect that the largest droplets will be in conditions such as (b) and (c) above while the smallest droplets can be expected to be in conditions such as (a) and (d).[46] In any case, the actual condition of the spray at the point of impingement with the preform is quite complex, and this is an area where more research work is required.

To calculate the temperature of a droplet of volume V_d as a function of the distance from the point of atomization, we assume that the spatial variations of the temperature inside the droplet can be neglected (lumped-parameter representation[34]). A simple heat balance equating the rate of change of the sensible and latent heats in the drop to the rate of heat extraction from the droplet surface by the atomizing gas gives

$$\rho_m V_d C_p \frac{dT}{dt} = h(T - T_o)A_d \qquad [8]$$

where

$$C_p = \begin{cases} C_{pl}, & \text{for } T > T_N \\ H^*/(T_R - T_S), & \text{for } T_S < T < T_R \\ C_{ps}, & \text{for } T < T_S \end{cases} \qquad [9]$$

is an effective specific heat.[36] The heat transfer coefficient h is estimated from the Ranz-Marshall correlation for the flow around spheres.[66] Once again, although work is required in order to verify the appropriateness of this assumption, it provides a simple means of estimating the heat exchange between droplets and gas.

It is well known[40] that when a solid phase nucleates inside an undercooled liquid drop, the droplet undergoes recalescence. Recalescence is simply the rapid rise in the droplet temperature resulting from, on the one hand, the rapid release of the latent heat of solidification, and, on the other, the inability of the surrounding gas to dissipate this energy outburst.[55] As the temperature of the droplet increases during recalescence, the rate of release of the latent heat decreases, and it becomes comparable to the rate of heat extraction by the gas when the so-called recalescence temperature is reached. This recalescence takes place within microseconds of the onset of nucleation, and it finishes when the rate of latent heat release becomes equal to the rate of heat extraction, *i.e.*,

$$H^* V_d \frac{df_s}{dt} = h(T_R - T_o)A_d \qquad [10]$$

Equation [9] can be used to calculate the maximum recalescence temperature T_R. The rate of increase of the fraction solidified during recalescence is assumed to be a linear function of the undercooling, *i.e.*[41]

$$\frac{df_s}{dt} = K(T - T_L) \qquad [11]$$

For the calculations described below, the nucleation temperature T_N has been considered part of the input data while the coefficient in Eq. [11] has been taken as given in Reference 37. As the results below will show, the fraction of solid formed in any given droplet during recalescence is not much different from 0.1. This is to be expected since the undercoolings assumed in our calculations were only between 20 and 40 °C. Therefore, further solidification of the droplets after recalescence occurs more like in conventional casting, and we can try to estimate the size scale of the resulting microstructure from standard correlations such as the one given in Reference 54.

Equations [1] through [11] constitute the mathematical formulation of the model of the atomization stage of the spray deposition process. It should be noted that a similar model has been independently developed and is described in Reference 44. Also, general modeling ideas that may be applicable to the analysis of spray deposition have been presented in Reference 38. Finally, a more involved computational study of the fluid flow phenomena in a somewhat related system has been presented in Reference 48.

B. *The Deposition Step*

In Section II.A, a methodology has been described which can be used to compute the thermal state of the atomized droplets at the moment of impact with the preform. In this section, we proceed to describe the second part of the mathematical model, namely, the computation of the temperatures and solidification rates in the growing preform during (and after) deposition. It should be noted that since the thickness of the preform is orders of magnitude larger than the diameter of typical droplets in the spray, spatial variations in the temperature across the deposit must be taken into account (*i.e.*, a distributed-parameter representation[34] is mandatory).

First, from an overall metal balance, the instantaneous deposit thickness is readily obtained as

$$X = (Q_m/\rho_m A_s)t \qquad [12]$$

The temperature distribution in the growing deposit is calculated from the differential thermal energy balance equation, assuming that heat conduction takes place only in the direction of the deposit thickness. Therefore, for the schematic arrangement shown in Figure 9, the energy equation is

$$\frac{\partial H}{\partial t} = \frac{\partial}{\partial x}\left(\frac{\partial u}{\partial x}\right) \qquad [13]$$

where

$$H = \begin{cases} (u - u_{LS})/\alpha_L + H_f, & \text{for } u > u_{LS} \\ (u/u_{LS})H_f, & \text{for } 0 < u < u_{LS} \\ u/\alpha_S, & \text{for } u < 0 \end{cases} \qquad [14]$$

and

$$u = \begin{cases} k_L(T - T_S), & \text{for } T > T_S \\ k_S(T - T_S, & \text{for } T < T_S \end{cases} \qquad [15]$$

and

$$u_{LS} = \bar{k}\,(T_L - T_S) \qquad [16]$$

The problem described by Eqs. [12] through [16] is subject to the following initial and boundary conditions:

(a) The temperature of the spray at the moment of the first impact on the substrate is given by the solution of the problem described in Section II.A above.

(b) At the preform-substrate interface, $x = 0$,

$$k\frac{\partial T}{\partial x} = h_{\text{bot}}\,(T - T_{\text{sub}}) \qquad [17]$$

(c) At the top surface of the deposit ($x = X$),

$$k\frac{\partial T}{\partial x} = (\bar{H} - H_{\text{top}})\,Q_m/A_s + h_{\text{top}}\,(T - T_o) + \sigma T^4 \qquad [18]$$

where the heat transfer coefficient for the convective exchange of energy between the chamber atmosphere and the top surface of the deposit, h_{top}, is assumed to be at least one order of magnitude smaller than h_{bot}. Also, the emissivity has been put equal to unity, and the temperature on the wall of the atomization chamber is assumed negligible in comparison with the temperature of the deposit. All these assumptions seem reasonable, but more work is required in order to verify their general applicability.

It should be noted that the first term on the right-hand side of Eq. [18] represents the heat input to the preform from the impinging spray and becomes equal to zero once deposition is over.

Equations [12] through [18] constitute the mathematical formulation of the model of the deposition stage in spray deposition. Together with Eqs. [1] through [11], the entire set of equations constitutes the model of the spray deposition process.

III. COMMENTS ON THE ASSUMPTIONS OF THE MODELS

In the previous section, the formulation of the mathematical model of the spray deposition process has been presented. However, little was said about the simplifying assumptions introduced in order to make the problem tractable. In this section we proceed to comment and discuss the most important assumptions. Since the model is composed of two parts (*i.e.*, the atomization step and the deposition step), the discussion of the assumptions is also presented in two parts.

A. *The Atomization Step*

A fine dispersion of droplets is formed when a liquid metal stream is impacted by high speed gas jets, and are rapidly quenched while in flight. In order to calculate droplet temperatures as functions of time, it is necessary to know the relative velocity between individual droplets and the gas. The relative velocity depends, in turn, on the size distribution of the droplets in the spray. The main assumptions made in the development of the first part of the model are as follows:

(a) The droplet size distribution in the spray is established immediately upon atomization, and it does not change afterward; therefore, the short period of time required for the disintegration of the molten stream is neglected. This assumption has been shown to be adequate, at least for the case of the ultrasonic gas atomization process.[45]

(b) The droplets acquire spherical shapes as soon as they form. It has been shown elsewhere[39] that this is indeed the case during liquid metal atomization due to the high surface energies characteristic of liquid metals.

(c) The droplets in the spray move in a rectilinear fashion driven by the combined effects of their own weights and of the acceleration forces exerted on them by the

moving gas. Therefore, the small amount of fluid adhered to the particle, which must also be accelerated, is neglected. Also, the dependence of the instantaneous acceleration on the state of development of the fluid motion around the spherical droplet is disregarded. These assumptions are harder to justify and more research work is needed in order to verify their appropriateness. However, based on prior experience with the use of Eq. [5], it is intuitively felt that results of the correct order of magnitude can still be obtained from it.

(d) The droplets are quenched during flight by the moving gas at a rate specified by a heat transfer coefficient. The value of this coefficient for a particular droplet is a function of the droplet size and of the relative velocity between the droplet and the gas phase. Moreover, the actual value of h can be estimated from the Ranz-Marshall correlation mentioned in Section II.A. This assumption is also hard to justify since the actual conditions during atomization can be different to those corresponding to the domain of validity of the correlation. The assumption is introduced here mainly as a last resort and in view of the lack of better alternatives. An attempt toward a more rigorous analysis of the heat transfer processes in two-phase sprays has been recently described;[48] such an approach is much more complicated than the one described here and necessarily involves longer computation times. Furthermore, the analysis presented in Reference 48 appears to be restricted to the case when the two phases in the spray possess similar physical properties, and this obviously excludes the gas-metal systems in which we are interested.

(e) The temperature gradient along the droplet radius is neglected. This implies that the droplet temperature is computed using a lumped-parameter model to represent the heat transfer process between droplet and gas. This assumption has been shown to be appropriate because of the smallness of the Biot number involved.[37] To illustrate this point, Figure 2 shows the temperature-time curves for three different particles calculated according to (i) a lumped parameter model, and (ii) a distributed-parameter model (*i.e.*, taking temperature gradients across the droplet into account). The distributed-parameter model uses a finite difference method to solve the differential thermal energy balance equation in spherical coordinates. The temperatures calculated for the three droplets from the two models are so close to each other that they cannot be resolved in this figure! The excellent agreement between the two models indicates that the temperature gradients across the droplet radius can be safely neglected for the droplet size ranges of interest. This is very advantageous since the lumped-parameter model is easier to program and much faster to execute in the computer.

B. *The Deposition Step*

The formulation of the deposit in spray deposition is accomplished by collecting the spray onto a suitably designed substrate. Fine, uniformly sized, low-segregation and equiaxed grains have been observed through the entire thickness of the deposit when the operation is performed correctly.[50–53] Excellent properties have been obtained in samples of several different alloys prepared by liquid dynamic compaction.[54–56] In order to effectively control the structure and the properties of the as-deposited material, it is necessary to understand the role of the processing variables. The mathematical model proposed here can be used, in conjunction with experiment, in order to obtain a better understanding of the role of processing on the properties. Since it is well known that thermal histories usually determine the microstructure of castings,[69] it is important to know the thermal history in the preform during spray deposition. Although conditions during spray deposition are quite different from those encountered during casting solidification, the knowledge of the temperature distribution during the formation of the preform is a necessary first step toward an understanding of the solidification process in the new process. Moreover, temperature measurements are relatively easy to perform and the results of such measurements can then be compared with the results of computer calculations.

The calculation of the temperature distribution in the deposit as a function of time can be carried out as described in Section II.B above. However, some comments are due regarding the simplifying assumptions introduced. These are:

(a) The deposition rate is assumed to be spatially uniform and independent of time. This assumption is made in order to simplify the analysis and because reliable measurements of this parameter do not seem to have been performed. In practice, the deposition rate is often nonuniform and also time dependent. However, uniformity can be approached by careful control of the process

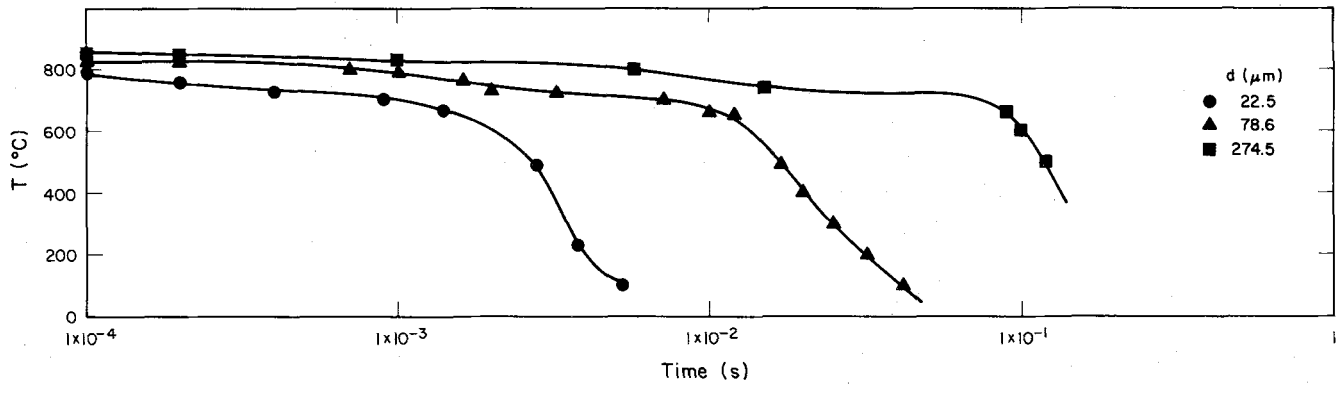

Fig. 2—Comparison of temperatures calculated according to a lumped-parameter model and distributed-parameter model for three typical droplets.

parameters.[57,58,59] This assumption is not vital for the model, and, if required, spatial and temporal variations in the deposition rate can be readily incorporated into the model. However, in particular, the incorporation of the spatial variation will significantly increase the computational task. Experimental work is also required in order to characterize the deposition rate.

(b) The transfer of heat through the deposit takes place only along the through-thickness direction (unidirectional) and is by conduction only. This seems justified since most of the thermal energy of the deposit is extracted by the substrate, and the temperature gradient across the deposit thickness is larger than along any other direction. This is also done for simplicity since the flows of heat on the plane of the preform can be readily incorporated into the model. The computational load, however, would be significantly increased.

(c) The rate of transfer of thermal energy from the spray into the deposit is directly related to the average enthalpy content of the spray at the moment of impact with the deposit. The average enthalpy content of the spray at the time of impact with the preform is simply the weighted average of the total heat content of each and every droplet in the spray. The total amount of heat contained within every droplet is calculated as described in Section II.A. This assumption is reasonable since the hot metal droplets constitute the most important source of heat for the deposit.

Besides the energy brought into the deposit by the metal drops, heat is lost from the top surface of the preform by convection into the gas phase and also by radiation into the atomization chamber walls. Our understanding of these heat transfer mechanisms during spray deposition is quite poor and only order of magnitude estimates are possible at this point. More experimental work is also required in this area in order to clarify the relative importance of these heat transfer mechanisms.

(d) The rate of heat transfer from the deposit into the substrate is assumed to be given by a heat transfer coefficient. Because of thermal stresses at the preform-substrate interface the thermal contact is expected to be significantly less than ideal (*i.e.*, at the interface, the substrate and the preform will have different temperatures). We are not aware of any measurements of this thermal resistance in a spray deposition system. However, there are some measurements available for castings systems with sections similar to the ones produced by spray deposition. Therefore, as a first approximation and in view of the lack of a better alternative, the value of the heat transfer coefficient at the substrate-preform interface has been taken from the compilation presented in Reference 60.

IV. COMPUTATIONAL CONSIDERATIONS

Computer programs have been prepared for the execution of the calculations required by Eqs. [1] through [18]. The programs have a modular structure; the two main modules being the calculation of the temperature in the droplets and the calculation of the temperature in the deposit. These two main programs can be used together or independently of each other. In order to understand the sequence of computation, one should concentrate on a given droplet formed at the atomization point (say d_{50}) and then follow its path as it travels down the atomization chamber. Once the droplet hits the substrate, it loses its identity and becomes part of the preform. The calculation then proceeds to find the temperature distribution in the preform.

For the calculations in the atomization stage, the droplet size distribution is first computed from Eqs. [1] through [4] using the data in Table I. Then, the droplet velocity is calculated as a function of the flight distance by numerical integration of Eq. [5]. Finally, the droplet temperature is obtained by solving Eqs. [7] through [11] numerically.[67] The calculation of the temperature of the various droplets stops when the distance traveled by them becomes equal to the separation between the atomization point and the collecting substrate. The average enthalpy content of the spray at impact is then calculated.

The calculation of the temperature distribution in the preform as a function of time is carried out by solving Eq. [13] subject to the constraints posed by Eqs. [11] and [14] through [18]. To solve Eq. [13] an explicit finite difference method is used.[68] In this method, the partial derivatives are approximated by finite differences ratios over a previously selected computational network of grid points. The calculation for the deposit proceeds as follows: first, an assumed initial deposit thickness x_o, not larger than 10 pct of the final preform thickness, is introduced and its temperature assumed equal to the temperature of the impinging spray. This artificial initial thickness is introduced in order to be able to use a relatively coarse computational grid. The finite difference analogue of Eq. [13] is then solved to obtain a new temperature profile in the growing preform. The calculation is repeated until the value of X from Eq. [12] becomes greater than X_o by one-half of the grid spacing. At this point, the deposit thickness is increased by one grid spacing and Eq. [13] solved in the now thicker deposit to obtain a new temperature profile. The calculation is repeated in this fashion until the end of deposition when the preform reaches its final thickness.

For reasons of numerical stability, the time step must be a quadratic function of the grid spacing.[68] Therefore, the finer the grid, the smaller the time step and the longer the computation. During the course of this investigation, it was found that 101 grid points across the final deposit thickness is the minimum number of points required in order to obtain reasonable accuracy. For the most part, the calculations reported below have been done using 201 grid points.

Typically, the calculation of droplet temperatures can be done in about 2 minutes in an IBM-XT computer, while the computation of the temperature field in the deposit requires about 30 minutes in either a MicroVax II or an Apollo Domain 3000 workstation.

V. RESULTS

Some results of computations carried out using the model described in Section II are presented in this section. In order to maintain coherency with the formulation, the results for the atomization step of the process

are presented first. Results of computations for the deposition step are presented in the second half of the section.

A. *The Atomization Step*

As the behavior of the various droplets is qualitatively similar and for brevity, only results for the particle of size d_{50} will be presented. Results for other particle sizes will be similar except for the difference in scale.

The computed velocity for a particle of size d_{50} is shown in Figure 3 together with the assumed gas velocity. As expected, the droplet is rapidly accelerated by the moving gas, although the rate of change of the velocity decreases as the droplet moves down. Once the maximum velocity is reached, the particle travels down at approximately constant velocity for a considerable distance. All droplet sizes exhibit qualitatively the same behavior but, of course, the smaller droplets accelerate faster initially. The values in Figure 3 can be compared with recent measurements reported in Reference 52. Although the results in Reference 52 were not available to us when the calculations were carried out, the calculated velocities appear to be of the same order of magnitude as the measured ones. However, the measured values are somewhat higher than the computed ones. Work is in progress to account for the discrepancy.

Figure 4 shows the computed heat transfer coefficient at the drop-gas interface for the same droplet as before. It is seen that the value of the coefficient decreases monotonically with the flight distance since the relative velocity between the gas and the drop also decreases.

Figure 5 shows the computed temperature as a function of the flight distance for the same droplet. There are four distinct regions in this curve. First, the temperature falls quite rapidly due to the intense quenching effect of the gas on the fully molten droplets. Then, the temperature rises sharply as nucleation and recalescence take place, and the liberated latent heat is released so fast that it cannot be dissipated by the cooling gas. After this, the temperature falls off again, this time at a somewhat slower rate, due to the release of the remaining latent heat contained in the droplet. Finally, once solidification is complete, the droplet temperature decreases rapidly again. These four stages can be more clearly appreciated in the cooling rate *vs* flight distance plot shown in Figure 6. It is seen there that the initial quenching rate of the liquid droplet is of the order of $2 * 10^5$ °C/second. This very high cooling rate turns into a heating rate which reaches up to about $2 * 10^6$ °C/second, when recalescence takes place upon nucleation of the solid phase. The temperature rise stops when the recalescence temperature, as given by Eq. [10], is reached. After that, solidification continues in the more conventional way (*i.e.*, on cooling), under a cooling rate of about $1 * 10^4$ °C/second. Finally, when solidification is complete, the cooling rate rises again somewhat, this time up to about $1 * 10^5$ °C/second. Note that for the calculations shown in Figures 3 through 6, the droplet is assumed to travel down the chamber for a distance of up to 1 m. Therefore, if a substrate were placed in the way of the flying droplet at a distance of, say 0.5 m from the atomization point, the droplet would be just about 100 pct solid at the time of impingement on the substrate.

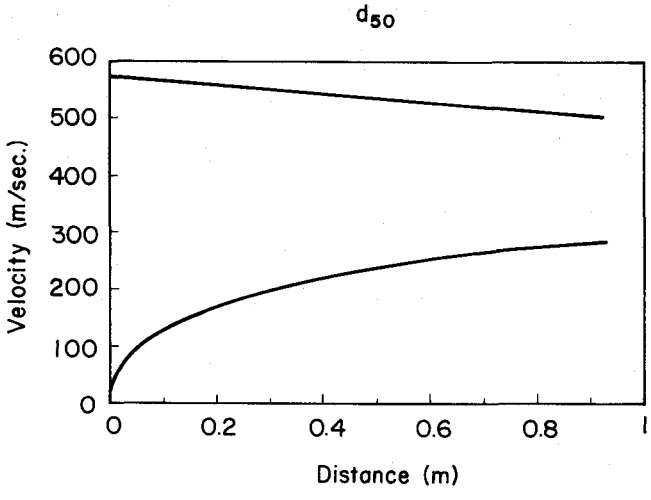

Fig. 3—Computed gas and droplet velocities for drop d_{50} as functions of distance along the atomization chamber.

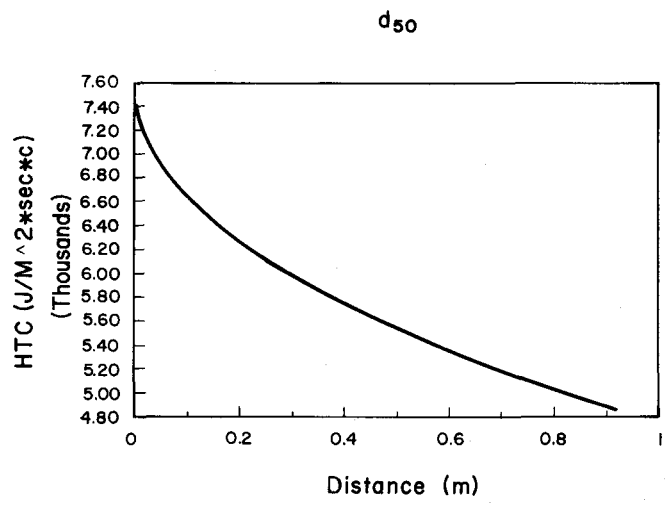

Fig. 4—Computed heat transfer coefficient from droplet d_{50} as a function of distance along the atomization chamber.

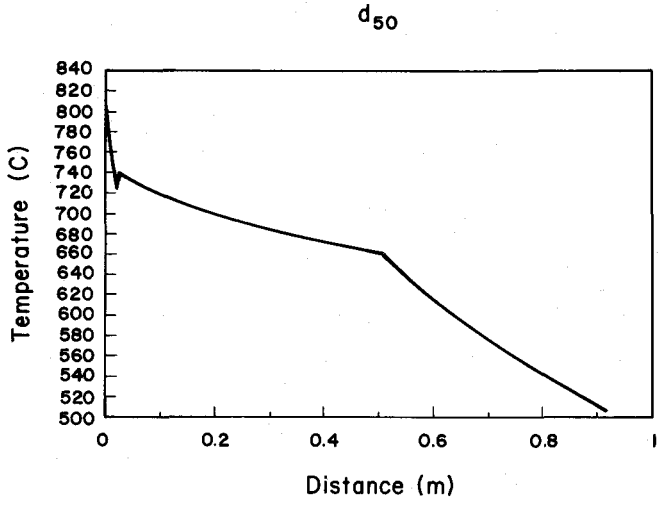

Fig. 5—Computed temperature for droplet d_{50} as a function of distance along the atomization chamber.

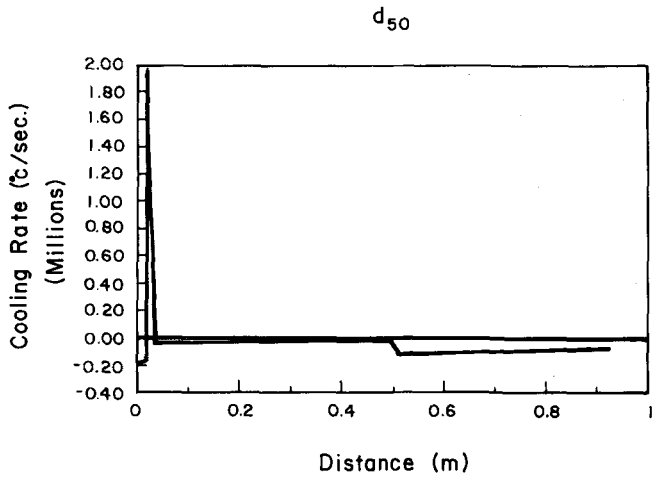

Fig. 6—Computed time rate of change of temperature for droplet d_{50} as a function of distance along the atomization chamber.

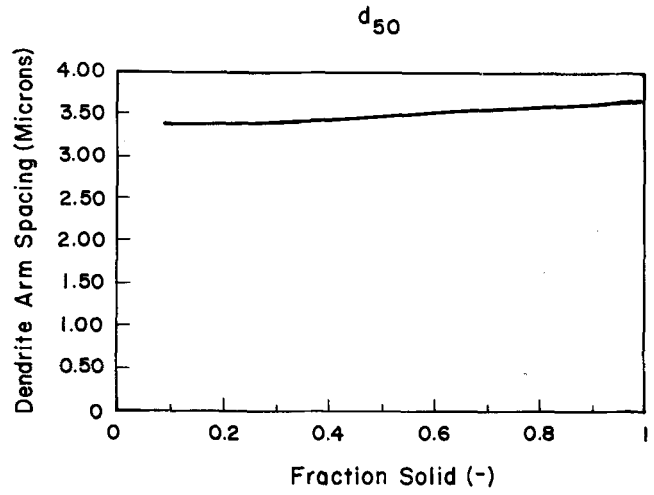

Fig. 8—Computed size of dendrite arm spacing as a function of the fraction solidified inside droplet d_{50}.

Although the behavior of droplets with sizes different from d_{50} is qualitatively similar, the calculations show that the smaller drops (*i.e.*, $d < d_{16}$) solidify entirely within the first few milimeters of flight, whereas the largest drops (*i.e.*, $d > d_{84}$) may even be fully molten after a flight distance of about 3 m.

From a practical standpoint, it is important to know the metallurgical condition of the droplets during flight, namely, the fraction solidified and the dendrite arm (or cell) spacing. Figure 7 shows the computed fraction of droplet that has solidified as a function of the flight distance. As expected, this is a monotonically increasing function since the droplet solidifies on cooling through the melting range. The curve indicates that the initial 10 pct of solid phase forms very rapidly, at a distance of about 0.2 m, during the recalescence following nucleation. Finally, Figure 8 shows the calculated dendrite/cell spacing in the flying droplet, from the empirical relation[54] $\lambda = 50\ (\dot{T})^{-0.3}$ and the cooling rate of about $1 * 10^4$ °C/second in Figure 6, as a function of the fraction of droplet that has solidified. For the droplet in question (d_{50}), the cell size of about 3 microns is nearly independent of the fraction solidified (and, thus, of the flight distance). Therefore, the cell size in the droplets which solidify in flight depends mostly on the droplet diameter. These predictions are in rough agreement with the results of experimental measurements.[49] For example, Figure 17 shows a 60-micron atomized alloy particle, obtained using the set-up shown in Figure 16, in which the dendrite (or cell) spacing is of the order of 2.5 microns.

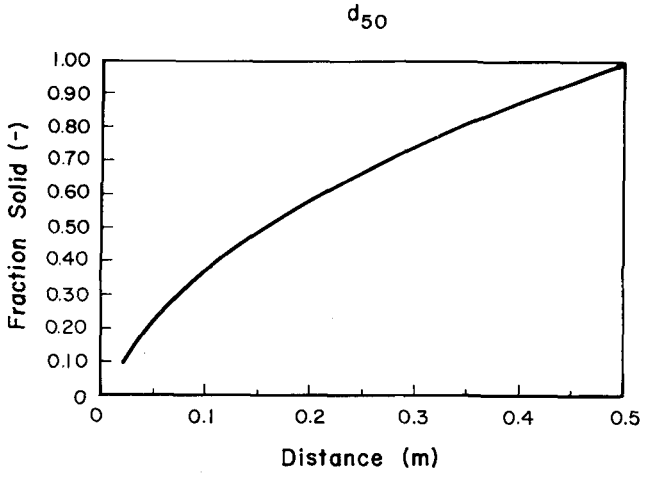

Fig. 7—Computed solidified fraction contained in droplet d_{50} as a function of distance along the atomization chamber.

B. *The Deposition Step*

A schematic representation of the deposition step in spray deposition is shown in Figure 9. It is seen that the spray of atomized droplets (some of them liquid, a few solid, and some in between) impinges on the partially grown deposit which in turn is being cooled from below by the substrate. Figure 10 shows the computed temperatures for two points in the preform as functions of time. Two main regions can be distinguished in these curves, especially in the one corresponding to the top surface of the deposit. These regions correspond to $t < t_{dep}$ and $t > t_{dep}$, respectively. While the spray is falling on the partially grown deposit (*i.e.*, for $t < t_{dep}$), the temperature of the top falls first and then rises during deposition. The temperature at the lower surface decreases continuously. Once deposition is over, the two temperatures fall relatively rapidly, and the temperature difference between top and bottom surfaces of the deposit is reduced. In all cases, however, the temperature does not rise too much above the solidus but hovers around this value (660 to 680 °C) until the end of deposition. A possible explanation for the temperature rise at the top surface of the deposit is that the rate of heat extraction by the substrate is marginally overcome by the rate of heat input due to the impinging spray as the preform grows. Note that the temperature at the top surface initially drops (for $t < 5$ seconds) and starts rising only when the deposit becomes thicker than about 4000 microns. The accumulated energy results in a mild, localized heating of the preform.

From the temperatures displayed in Figure 10, one can readily calculate the corresponding cooling (heating) rates

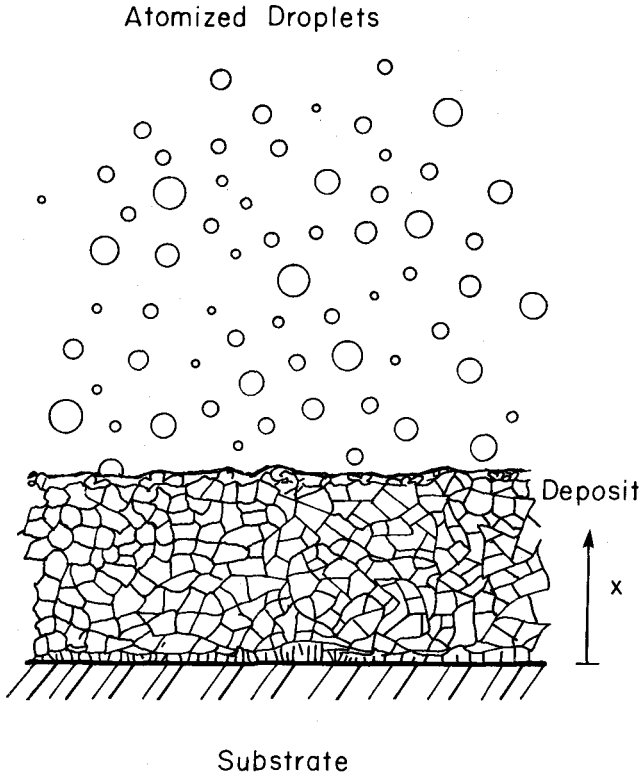

Fig. 9—Schematic representation of the deposition stage of the SD process.

at various points in the deposit as functions of time. Figure 11 shows the computed time rates of change of the temperatures for the top and bottom surfaces of the deposit. The two characteristic regions mentioned before can also be seen in this plot., *i.e.*, the regions for $t < t_{dep}$ and $t > t_{dep}$, respectively. A striking feature of these curves is that the computed cooling rates during solidification (*i.e.*, for $18 < t < 22$ seconds –lower curve– and for $31 < t < 37$ seconds, –top curve–) are of the order of 1 to 10 °C/second and, therefore, are much smaller than the rates calculated for typical droplets in the spray. Of course, much faster rates are calculated during the first few milliseconds of deposition, but they are short-lived. The much lower rates calculated in the preform in comparison with those in the droplets are perhaps to be expected since the characteristic heat transfer dimension in the droplets (*i.e.*, the radius) is several orders of magnitude smaller than the thickness of the preform.

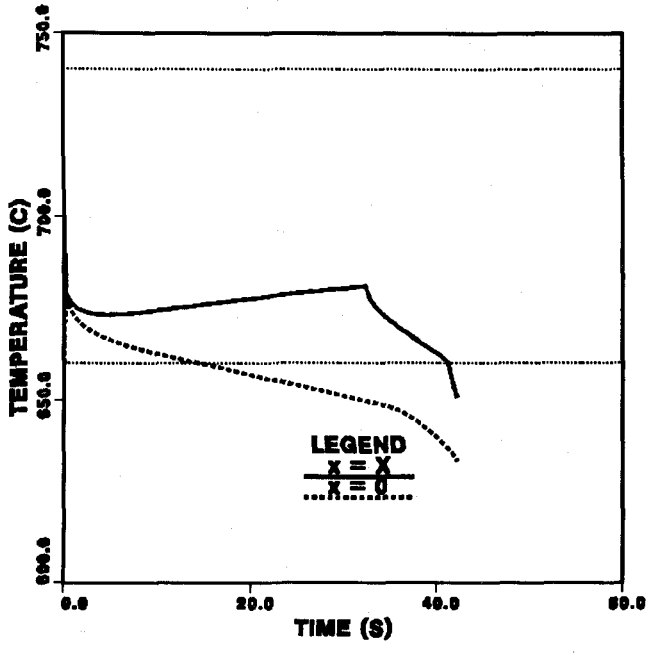

Fig. 10—Computed temperature histories for two points in the deposit.

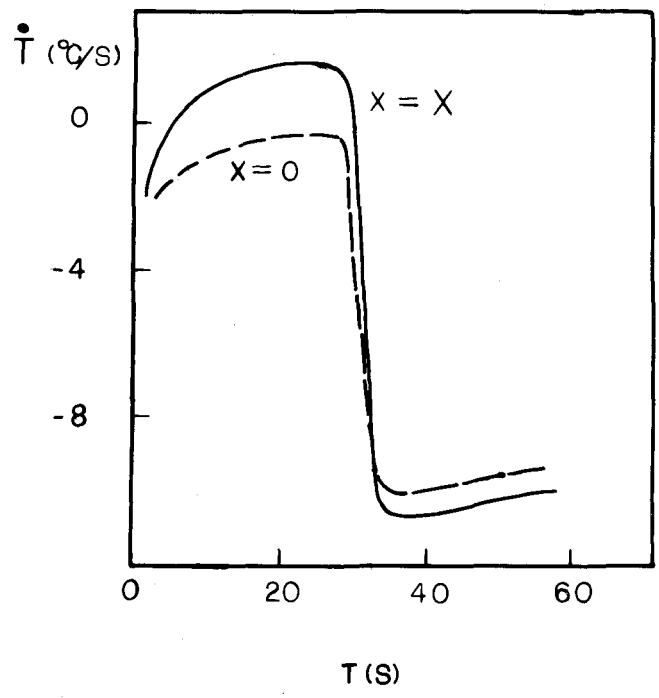

Fig. 11—Computed cooling rates for upper and lower surfaces of deposit.

Even after completion of the solidification, when the computed cooling rates are highest, the values are only about 100 °C/second. Of course, the microstructure of the as-deposited preform is a result of the solidification process, and the cooling rates in the solid state have a negligible effect on it. Prior microstructural observations of as-deposited preforms have produced grain sizes such as those shown in Figure 12, *i.e.*, between 6 and 25 microns.[49] Using $\lambda = 50\ (\dot{T})^{-0.3}$, one obtains 1173 and 10 °C/second for the grain sizes indicated. These cooling rates during solidification, estimated from the microstructure, are up to three orders of magnitude larger than the ones predicted by the model! Other microstructural features, such as the reduced segregation and the equiaxed nature of the grains, also suggest that the solidification times are much smaller than what the calculations suggest. This evidence has been used to support the claim that the spray deposition process is just another rapid solidification technique.[16]

Alternatively, one can argue that what is unexpected is the reduced segregation and fine grains typical of spray-deposited preforms. As mentioned before, the characteristic distance for heat transfer in the preform is of the order of centimeters, and it is well known that one can not achieve cooling rates in excess of 10^3 °C/second when

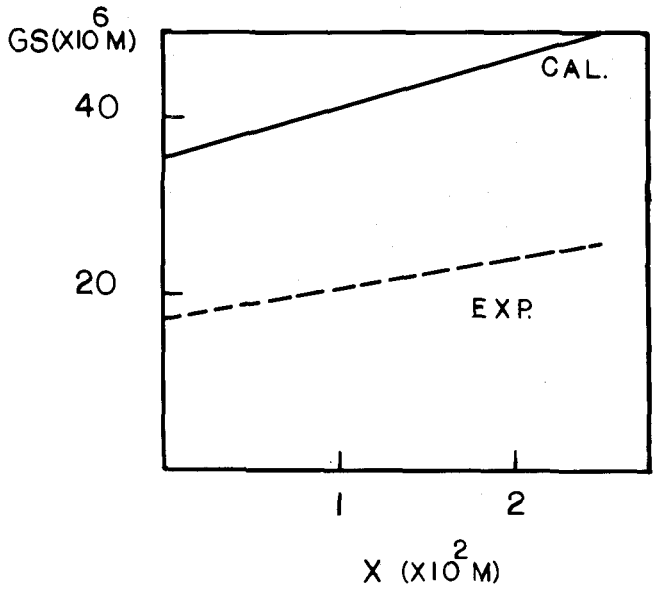

Fig. 12—Comparison of computed and measured grain sizes across the deposit thickness. Measurements are from Ref. 49.

the section to be cooled is thicker than about 10 mm. Therefore, it would seem that the cooling rates estimated from the microstructure are in contradiction with established heat transfer theory. However, it should be noted that when a single droplet impacts the growing preform, it loses heat at a rate much faster than the cooling rate of the preform at the top surface. It must be recognized that the SDP has some unique features.

On the one hand, the process makes use of atomized droplets which, because of their small sizes, cool very rapidly. On the other hand, the process produces bulk shapes with sections not very different from those that can be produced by more conventional casting techniques. In this sense, spray deposition brings together, in the same process, features of rapid solidification and features of conventional casting. In doing this one avoids some of the most important limitations of those processes as thick sections with fine grains and reduced segregation can be produced in a single operation. The cooling rates during solidification calculated using the model are indeed similar to the values encountered during processes such as die-casting and thin slab casting. The resulting as-deposited microstructures, on the other hand, are similar to those obtained by rapid solidification processing. The computed results would suggest that the process actually operates instead under a cooling regime which has been designated as medium rapid.[61] Recent experimental measurements of preform temperature during deposition[62] have produced cooling rates during solidification which are very close to the ones predicted by the model.

The temperature measurements reported in Reference 62 suggest another possible explanation for the large discrepancy between the computed cooling rates and the cooling rates derived from microstructural measurements in as-deposited preforms. For the temperature measurements, Bewley *et al.* used simply a thermocouple embedded in the growing preform. It is clear that the temperature recorded by the thermocouple is really an average value over the volume occupied by the hot junction; *i.e.*, temperatures in volumes smaller than this hot junction volume cannot be measured with this instrument and a finer junction is required. A very similar situation is encountered when doing numerical calculations. The resolution of the calculation is limited by the size of the grid employed. For a grid consisting of 201 points in a 0.0254 m thick preform, the grid spacing is 127 microns. Therefore, if there were temperature variations in the deposit over distances smaller than 254 microns, these would not be detected by the calculation. Now, since a 100-micron diameter droplet turns into a 5 to 10 micron thick pancake when it strikes a solid surface,[71] it is easy to see that the computed temperature at a grid point really represents some sort of average over many such pancakes. Therefore, the thermal histories of individual pancakes cannot be resolved by the computation. However, the thermal history of the process depends strongly on the thermal behavior of these individual pancakes which are not being considered by the model! This fact alone can explain the discrepancy between predictions and measurements. Obviously, more work is needed in order to resolve this difficulty.

Figure 11 also shows that the cooling rates as functions of time (including during solidification), for the top and bottom surfaces of the preform (and, of course, for all points in between) are quite similar to each other. This would indicate that the thermal histories of various points in the preform are all very similar. Therefore, the solidification time is also very similar everywhere in the preform, and one can expect the microstructure as well to be quite similar from point to point. This homogeneity of the microstructure is indeed one of the most attractive features of spray deposition.[70]

Once the thermal history of the deposit has been determined, one can try to estimate the size of the microstructural features (*i.e.*, grains) from the cell size/cooling rate correlation, as was done in the case of the atomized droplets. Figure 12 shows a comparison between the computed grain size and the grain size measured in a typical deposit produced by the liquid dynamic compaction process developed at MIT. The curve shows that the grain size of preforms increases monotonically with distance from the substrate at a rate of about 300 microns/m. This is a rather small rate of increase, indicating that the microstructure is quite uniform across the preform thickness.

Although the computed grain size increases with distance at a rate approximately equal to the measured values, the actual grains are about half as large as the predicted grain size! This is the same discrepancy between model and experiment mentioned before, but this time in terms of the grain size rather than in terms of the temperature.

If we assume that the calculated cooling rates and solidification times are of the correct order of magnitude, this would indicate that perhaps the thermal history is not the only factor determining the final grain size in deposited preforms.

In order to show that factors other than the cooling rate during solidification may be important in determining the structure, Figure 13 shows the evolution of the isofraction solid lines in the preform during (and after)

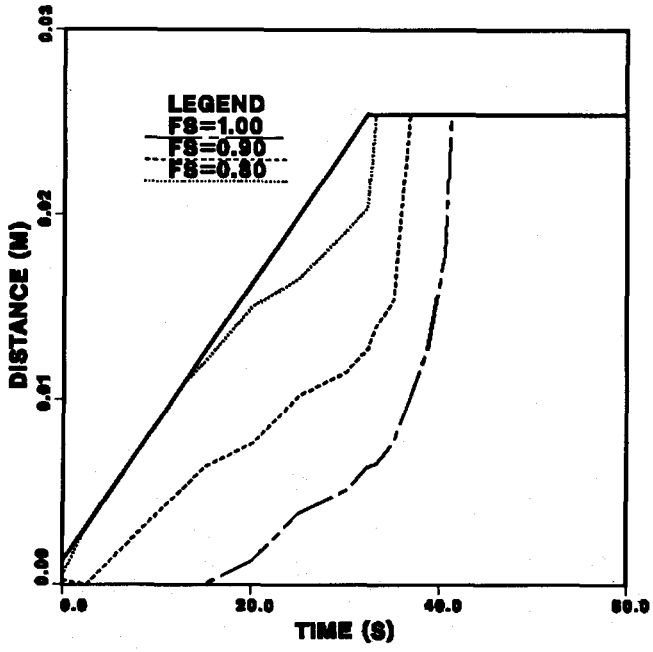

Fig. 13—Computed isofraction solid curves.

deposition. These curves are obtained from the temperature profiles in Figure 10 by assuming that the fraction solidified at any given point in the preform is equal to $(T_L - T)/(T_L - T_S)$. As seen also in Figure 10, Figure 13 shows that the top layers of the preform contain a small amount of liquid which increases gradually with time and reaches a value of about $f_L = 0.25$ toward the end of deposition.

First, during the initial stages of deposition (*i.e.*, for $t < 15$ seconds), the top portion of the deposit consists of a mushy region with a high content of solid and of approximately constant thickness. During the second part of the deposition stage (*i.e.*, for $15 < t < 30$ seconds), the thickness of the mushy zone increases rapidly and the proportion of solid phase inside it decreases, especially at the very top of the deposit. However, for the conditions of this calculation, the fraction solid at the top surface of the deposit never goes below 0.75. Finally, once deposition is complete (for $t = 30$ seconds), the mushy zone contracts and disappears in a few seconds, leaving a fully solidified deposit.

It is quite possible that the partially solidified grains present in the mushy region are not able to grow as large as the prevailing solidification time would allow. This may be so since the solid material in the mush is in the form of an interconnected network, which contains tiny pools of liquid in the interstitial spaces. The maximum size that the grains can attain under these conditions is restricted by the size of the pockets of liquid. The size of these pockets depends in turn on the size of the bits of solid present in the mush as well as on the total fraction of solid phase. Finally, the size of the bits of solid in the mush is a function of the size of the solid grains in the atomized droplets at the time of impingement. Although perhaps many of the droplets in the spray will be fully liquid at the time of impact with the preform, the smaller droplets (say $d < 20$ microns) most likely will be fully solidified by the time they hit the preform. For the conditions assumed in our calculations, even droplets as large as d_{50} will contain significant amounts of solid phase at the time of impact with the preform.

It should be stressed that the results described by Figures 10 through 12 correspond to a specific set of process variables, given by the values in Table I. Numerical experiments using, for example, a larger value of h_{bot} lead to preform top surface temperatures which stay below the solidus throughout deposition. Experimental measurements of preform temperatures as well as of the heat transfer coefficient at the substrate-preform interface are absolutely necessary in order to compare the predictions of the model with reality.

The model can be useful in the investigation of the effects of changes in the process parameters on the nature of the resulting deposits. For example, Figure 14 shows the calculated temperature profiles through the deposit thickness as functions of time for the case when the average enthalpy of the impinging spray is 50 pct larger than in Figures 12 and 13. As expected, the increased thermal energy content of the spray in this case results in higher deposit temperatures both during and after deposition. Although the computed behavior is qualitatively very similar to the one described before, the time for complete solidification is significantly delayed. The increased enthalpy content of the spray has also an effect on the final structure of the as-deposited preform. Since the mushy zone now spans almost the entire thickness of the deposit and because of the smaller fraction of solids at the top, the microstructure can be expected to be less uniform, coarser, and, in general, of a lower quality. Note, in particular, that the collapse of the mushy zone at the end of deposition now takes almost twice as long as in the previous case.

The average enthalpy content of the spray at impact is directly related to the nozzle-substrate separation (Figure 5), and the results indicate that the thermal history

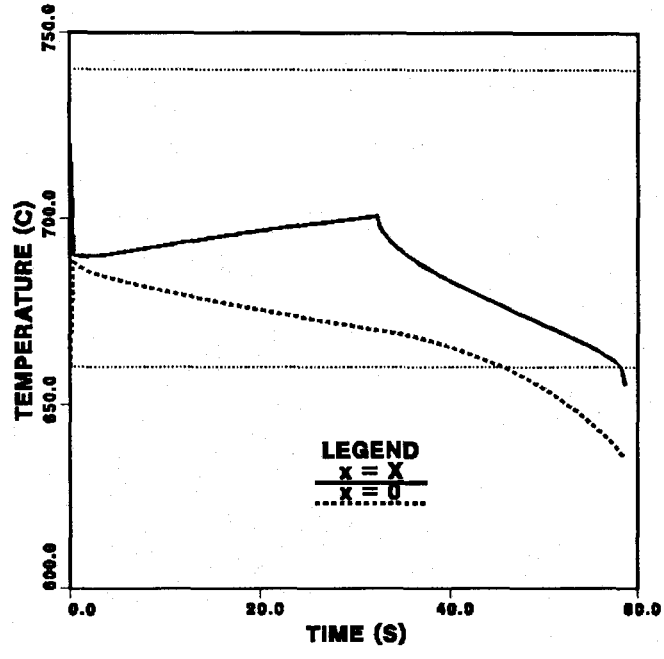

Fig. 14—Computed thermal histories for the case of large spray enthalpy.

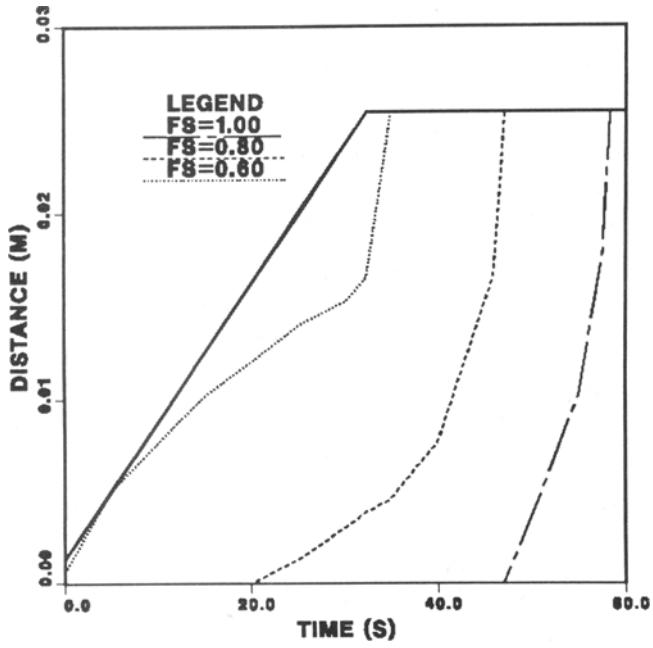

Fig. 15—Computed isofraction solid lines for the case of large spray enthalpy.

of the deposit will be dependent strongly on the value of this separation. This is hardly unexpected, but the extreme sensitivity of the results to the value of this parameter is an indication of its importance.

VI. DISCUSSION

A mathematical representation has been developed to describe the temperatures, cooling and freezing rates, and the microstructures obtained in the droplets and in the deposits formed during spray deposition. The first part of the model calculates the thermal histories for the atomized droplets while in flight, whereas the second part addresses temperatures in the growing deposit.

The model equations are highly simplified (a lumped-parameter-model and empirical correlations are used for the droplet computations, and one-dimensional conduction with change of phase is assumed for the deposit).

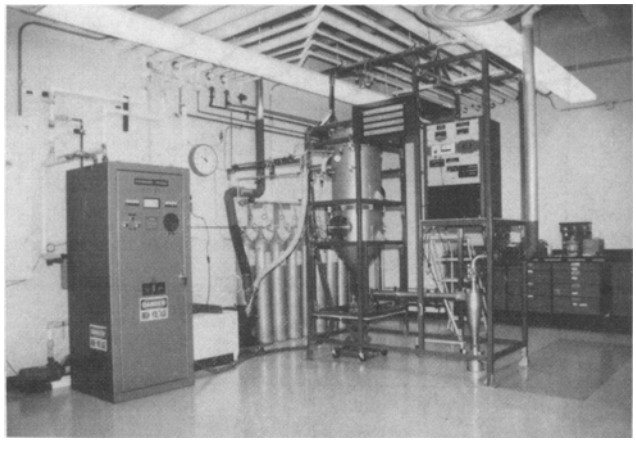

Fig. 16—Spray deposition facility at the Department of Mechanical Engineering of the University of California, Irvine.

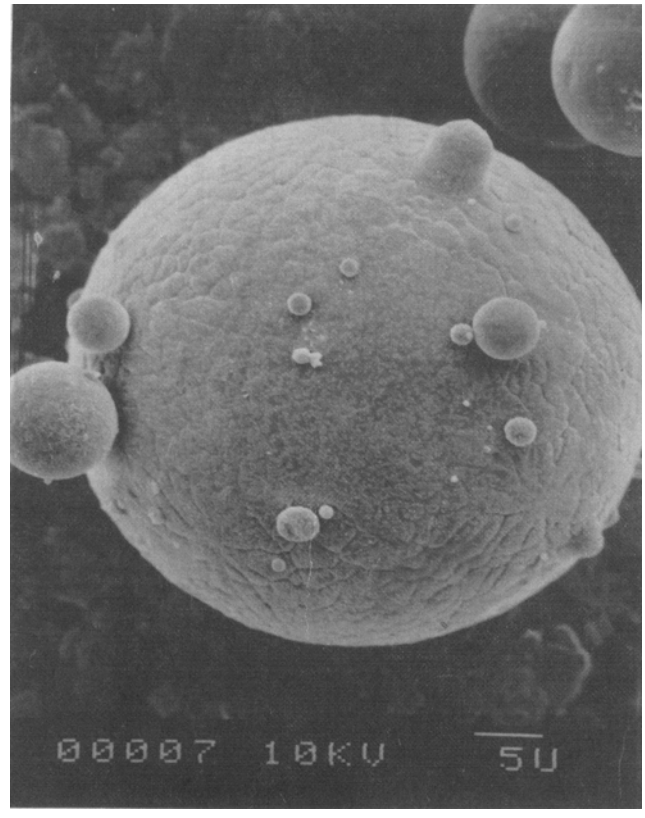

Fig. 17—Representative atomized powder obtained in the set-up shown in Fig. 16.

Nevertheless, the computed results have provided useful, hitherto not available insight into the behavior of spray deposition processes.

The principal findings of the work may be summarized as follows:

(1) When the process is properly controlled, there is a good balance between the rate of heat supply from the droplets in the spray on the one hand and the heat removal by the substrate on the other. Under these conditions, the cooling rates are relatively uniform through the entire deposit thickness, giving a more or less spatially uniform grain size, a highly desirable feature. This finding has been verified experimentally (Figure 12).

(2) The temperature history of the deposit is dependent very markedly on the average enthalpy of the arriving metal drops. Even small changes in the value of this enthalpy can give rise to very marked variations in the temperature profiles, in the extent of fractional solidification, and on the performance of the process in general.

(3) The theoretically predicted cooling rates during the solidification of the deposit were found to be of the order of 1 to 10 °C/second. These are in good agreement with the experimental measurements of Bewley *et al.*,[62] but are up to three orders of magnitude smaller than commonly accepted cooling rates derived from microstructural measurements. Indeed, the cooling rates found for spray deposition in this study are comparable to those encountered in processes such as thin-strip casting and die-casting.

(4) Upon calculating the grain size from the cooling rate

using conventional correlations, it was found that this, while giving the correct slope in relation to the deposit thickness, overestimated the size by about a factor of two. This apparent discrepancy may be explained by the fact that here we are not dealing with the solidification of an unconstrained melt, but have to be concerned with a rather more complex situation. Specifically, we have to deal with the freezing of a melt which contains partially solidified droplets and, hence, an appreciable fraction of solids. As discussed above, during their flight the smaller drops will partially or fully solidify at very high cooling rates, which would give dendrites of the order of a few microns. The end result is a solid, with a grain size which is an intermediate between these two extremes; that is, the dendrites contained in the partially solidified droplets and the equiaxed grains that would be produced in the preform if they were allowed to grow unhindered during the time available for solidification. Clearly, the analysis that has been presented must be regarded as a first step in the study of this rather complex process.

VII. CONCLUSIONS

The principal practical conclusions that may be drawn from this work are the following:

1. When properly controlled, the spray deposition process has the potential of producing solid deposits with a relatively uniform grain size through the thickness. The grains in the deposit are equiaxed and relatively free of segregation.
2. For the process to be successful the rate of heat supply and the rate of heat removal have to be balanced carefully; indeed the performance of the process appears to depend quite critically on the ability to control the enthalpy of the (partially solidified) droplets in the impinging spray.
3. Computer programs based on the model described are now available and can be useful both in the designing and in the operation of actual spray deposition systems.
4. Further work would be desirable in the following two areas:
   (a) The development of a better understanding of droplet formation and heat transfer in the spray in general, and
   (b) A better mathematical representation of the solidification process in the droplets and in the deposit.
5. It would be interesting to try to extend the usage of spray deposition into the production of other difficult-to-produce materials. A case in point would be the deposition of metal-matrix composites.[74]

NOMENCLATURE

a	coefficient in cell size–cooling rate correlation	(micron/(°C/sec)^b)
A_d	droplet surface area	(m^2)
A_o	cross-sectional area of metal jet	(m^2)
A_s	area of substrate	(m^2)
A_t	effective throat area of gas nozzle	(m^2)
b	exponent in cell size–cooling rate correlation	(−)
C_{drag}	drag coefficient for motion of sphere in fluid	(−)
C_D	discharge coefficient from crucible	(−)
C_p	specific heat	(Joule/kg °C)
C_{pl}	specific heat of liquid	(Joule/kg °C)
C_{ps}	specific heat of solid	(Joule/kg °C)
d_{16}	droplet diameter equal to the upper bound of 16 pct of the droplets	(m)
d_{50}	mass mean droplet diameter	(m)
d_{84}	droplet diameter equal to the upper bound of 84 pct of the droplets	(m)
d_o	diameter of molten metal stream from the crucible	(m)
f_s	fraction solid	(−)
g	gravitational constant	(m/sec^2)
h	heat transfer coefficient between droplets and gas	(W/m^2 °C)
h_{bot}	heat transfer coefficient at deposit-substrate interface	(W/m^2 °C)
h_{top}	heat transfer coefficient at the top surface of deposit (after the end of deposition)	(W/m^2 °C)
h_c	height of melt in crucible	(m)
H	enthalpy	(Joule/kg)
$\bar{H}$	average enthalpy of impinging spray	(Joule/kg)
H^*	fraction of latent heat remaining at the end of recalescence	(Joule/kg)
H_f	latent heat of fusion	(Joule/kg)
J_{gas}	gas flow rate	(kg/sec)
J_{melt}	melt flow rate	(kg/sec)
k	thermal conductivity	(W/m °C)
$\bar{K}$	average thermal conductivity of metal	(W/m °C)
k_L	thermal conductivity of liquid	(W/m °C)
k_S	thermal conductivity of solid	(W/m °C)
K	kinetic growth coefficient for undercooled solidification	(m/sec °C)

K_d	coefficient in powder size correlation	(−)
N_{Bi}	Biot number ($=hr_d/k$)	(−)
N_{Re}	Reynolds number ($=2 r_d \rho_g v_g/\mu_g$)	(−)
p_o	plenum pressure of atomizing gas	(Pa)
Q_m	deposition rate	(kg/sec)
r_d	droplet radius	(m)
t	time	(sec)
t_{dep}	deposition time	(sec)
T	temperature	(°C)
T_o	temperature of gas	(°C)
T_L	liquidus temperature	(°C)
T_N	nucleation temperature	(°C)
T_R	maximum recalescence temperature	(°C)
T_S	solidus temperature	(°C)
T_{sub}	substrate temperature	(°C)
$\dot{T}$	time rate of change of temperature	(°C/sec)
u	transformed temperature	(W/m)
v_d	droplet velocity	(m/sec)
v_g	gas velocity	(m/sec)
V_d	droplet volume	(m^3)
x	vertical distance in the deposit (measured from the substrate-preform interface	(m)
X	instantaneous deposit thickness	(m)
z	vertical distance (measured downward from the point of atomization	(m)
α	thermal diffusivity	(m^2 sec)
γ	C_p/C_v for atomizing gas	(−)
ΔT_s	initial melt superheat	(°C)
ΔT_u	maximum droplet undercooling	(°C)
λ	dendrite arm (or cell) spacing	(micron)
σ	Stefan-Boltzmann radiation constant	($W/m^2 K^4$)
σ_m	melt surface tension	(kg/sec^2)
ρ_d	droplet density	(kg/m)
ρ_g	gas density	(kg/m)
ρ_m	melt density	(kg/m^3)
η_g	kinematic viscosity of gas	(m^2/s)
η_m	kinematic viscosity of melt	(m^2/s)
μ_g	gas viscosity	(kg/m sec)
μ_m	melt viscosity	(kg/m sec)

Subscripts

l, L	liquid
s, S	solid

ACKNOWLEDGMENTS

E.G.-M. thanks the National University of Mexico for continued support and the Hartford Graduate Center for the provision of computing facilities. E.J.L. and N.J.G. express their gratitude for financial support to the Army Materials Research Laboratory, the Aluminum Company of America, Reynolds Metals, Department of Energy, Army Research Office, and to the NSF-MRL for permission to use their excellent facilities. Last but not least, we thank our reviewers for their many useful comments.

REFERENCES

1. G. Hildeman and M.J. Koczak: *Journal of Metals*, Aug. 1986, vol. 38, no. 8, pp. 30-32.
2. A. Lawley: *Journal of Metals*, Aug. 1985, vol. 37, no. 8, pp. 15-25.
3. S.J. Savage and F.H. Froes: *Journal of Metals*, Apr. 1984, vol. 36, no. 4, pp. 20-33.
4. V.W.C. Kuo and E.A. Starke, Jr.: *Metall. Trans. A*, 1985, vol. 16A, pp. 1089-103.
5. E.J. Lavernia, G. Rai, and N.J. Grant: *Journal of Materials Science and Engineering*, 1985, vol. 79, no. 2, pp. 211-21.
6. J.P.H.A. Durand, R.M. Pelloux, and N.J. Grant: *Materials Science and Engineering*, 1976, vol. 23, pp. 247-56.
7. P.K. Domalavage, N.J. Grant, and Y. Gefen: *Metall. Trans. A*, 1983, vol. 14A, pp. 1599-608.
8. E. Lavernia, B. Poggiali, I. Servi, J. Clark, F. Katrak, and N.J. Grant: *Journal of Metals*, Nov. 1985, vol. 37, no. 11, pp. 272-79.
9. Y.W. Kim, W.M. Griffith, and F.H. Froes: *Journal of Metals*, Aug. 1985, vol. 37, no. 8, pp. 27-33.
10. W. Wang and N.J. Grant: *International Journal of Rapid Solidification*, 1984, vol. 1, pp. 157-71.
11. N.J. Grant, S. Kang, and W. Wang: in *Aluminum Lithium Alloys*, T.H. Sanders, Jr. and E.A. Starke, Jr., eds., AIME, New York, NY, 1987, pp. 171-88.
12. R.K. Dube: *Powder Metallurgy International*, 1982, vol. 14, p. 108.
13. R.G. Brooks, C. Moore, A.G. Leatham, and J.S. Coombs: *Powder Metallurgy*, 1977, vol. 2, pp. 100-02.
14. B. Williams: *Metal Powder Report*, 1980, vol. 10, pp. 464-66.
15. R.H. Bricknell: *Metall. Trans. A*, 1986, vol. 17A, pp. 583-90.
16. E.J. Lavernia and N.J. Grant: *International Journal of Rapid Solidification*, 1986, vol. 2, no. 2, pp. 93-106.
17. E.J. Lavernia, G. Rai, and N.J. Grant: *International Journal of Powder Metallurgy*, 1986, vol. 22, no. 1, pp. 9-16.
18. K. Ogata, E.J. Lavernia, G. Rai, and N.J. Grant: *International Journal of Rapid Solidification*, 1986, vol. 2, no. 1, pp. 21-35.
19. T.S. Chin, Y. Hara, E.J. Lavernia, R.C. O'Handley, and N.J. Grant: *Journal of Applied Physics*, 1986, vol. 59, no. 4, pp. 1297-300.
20. E.J. Lavernai, T. Ando, and N.J. Grant: *Proceedings of the ASM's International Conference on Rapidly Solidified Materials*, P. Lee and R. Carbonara, eds., *ASM*, Metal Park, OH, 1986, pp. 29-44.
21. P.J. Meschter, R.J. Lederich, J.E. O'Neal, E.J. Lavernia, and N.J. Grant: *Annual Meeting of The Metallurgical Society*, New Orleans, LA, March 2-6, 1986.
22. J.M. Nell, G. Rai, E.J. Lavernia, and N.J. Grant: *Proceedings of the 1986 Annual Powder Metallurgy Conference and Exhibition*, Boston, MA, May 18-21, 1986.
23. T.W. Clyne, R.A. Ricks, and P.J. Goodhew: *International Journal of Rapid Solidification*, 1984, vol. 1, no. 1, pp. 59-80.
24. E.J. Lavernia and N.J. Grant: *Metal Powder Report*, April 1986, vol. 41, no. 4, pp. 255-60.
25. H. Lubanska: *Journal of Metals*, 1970, vol. 22, pp. 45-49.
26. G. Rai, E.J. Lavernia, and N.J. Grant: *Journal of Metals*, Aug. 1985, vol. 37, no. 8, pp. 22-26.
27. G.H. Geiger and D.R. Poirier: *Transport Phenomena in Metallurgy*, Addison-Wesley, Reading, MA, 1973, p. 135.

28. E.J. Lavernia, J. Nell, and M. Veistinen: *International Journal of Powder Metallurgy*, in press.
29. U. Backmark, N. Backstrom, and L. Arnberg: *Internal Report No. IM 1929*, Swedish Institute for Metals Research, Stockholm, Sweden, 1985.
30. J.A. Beattle and H.P. Julien: *Industrial and Engineering Chemistry*, 1954, vol, 46, no. 8, pp. 1668-69.
31. A.R.E. Singer, J.S. Coombs, and A.G. Leatham: in *Modern Developments in Powder Metallurgy*, H.H. Hausner and W.E. Smith, eds., Plenum Press, New York, NY, 1974, vol. 8, pp. 263-80.
32. J. Szekely: *Fluid Flow Phenomena in Metals Processing*, Academic Press, NY, 1979, p. 261.
33. H. Kurten, J. Raasch, and H. Rumpf: *Chemie-Ingenieur-Technik*, 1966, vol. 38, no. 9, pp. 941-48.
34. D.M. Himmelblau and K.B. Bischoff: *Process Analysis and Simulation; Deterministic Systems*, John Wiley and Sons, NY, 1968, p. 43.
35. J. Szekely and N.J. Themelis: *Rate Phenomena in Process Metallurgy*, John Wiley and Sons, NY, 1971, pp. 107-207; p. 611.
36. J. Szekely: in *Rate Processes of Extractive Metallurgy*, H.Y. Sohn and M.E. Wadsworth, eds., ch 5, Plenum Press, NY, 1979, pp. 429-63.
37. C.J. Levi and R. Mehrabian: *Metall. Trans. A*, 1982, vol. 13A, pp. 221-34.
38. T.W. Clyne: *Metall. Trans. B*, 1984, vol. 15B, pp. 369-82.
39. O.S. Niripochenko and Y.I. Naida: *Poroshykovaya Metallurgiya*, Oct. 1968, vol. 70, no. 10, pp. 1-3.
40. W. Gill, J.H. Yang, J.C. Mollendorf, and C.M. Adam: *Journal of Crystal Growth*, 1984, vol. 66, pp. 351-68.
41. S.R. Coriell and D. Turnbull: *Acta Metall.*, 1982, vol. 30, pp. 2135-39.
42. H. Jones: *Rapid Solidification of Metals and Alloys*, The Institution of Metallurgists, London, 1982.
43. T.R. Anantharaman and K. Suryanarayana: *Journal of Materials Science*, 1971, vol. 6, pp. 1111-35.
44. G. Gillen, P. Mathur, D. Apelian, and A. Lawley: *Proceedings of the 1986 Annual Powder Metallurgy Conference and Exhibition*, Boston, MA, May 18-21, 1986.
45. N.J. Grant: *Journal of Metals*, 1983, vol. 35, no. 1, pp. 20-27.
46. J.H. Perepezko and J.S. Paik: in *Rapidly Solidified Amorphous and Crystalline Alloys*, B.H. Kear, B.C. Giessen, and M. Cohen, eds., North-Holland, NY, 1982, pp. 49-63.
47. Y.I. Naida, V.S. Ivanov, S.F. Fedorov, and R.B. Manasyan: *Poroshkovaya Metallurgiya*, April 1980, vol. 208, no. 4, pp. 1-4.
48. P.G. Enright, L. Katgerman, J.C. Ludwig, and S. Rogers: *International Journal for Numerical Methods in Engineering*, 1987, vol. 24, pp. 231-49.
49. E.J. Lavernia: Ph.D. Thesis, Massachusetts Institute of Technology, Cambridge, MA, 1986.
50. E.J. Lavernia and N.J. Grant: *Proceedings of the Sixth International Conference on Rapidly Quenched Metals*, Montreal, Canada, Aug. 3 through 7, 1987. Also in *Materials Science and Engineering*, in press.
51. A.R.E. Singer and R.W. Evans: *Metals Technology*, Feb. 1983, vol. 10, pp. 61-68.
52. J. Lui, L. Arnberg, N. Backtrom, H. Klang, and S. Savage: *Proceedings of the Sixth International Conference on Rapidly Quenched Metals*, L'Universite de Montreal and McGill University, Montreal, Canada, Aug. 1987.
53. M. Veistinen, E.J. Lavernia, Y. Hara, R.C. O'Handley, and N.J. Grant: *Proceedings of the Spring Meeting of the Materials Research Society*, Anaheim, CA, 1987.
54. H. Matyja, B.C. Giessen, and N.J. Grant: *Journal of the Institute of Metals*, 1968, vol. 96, pp. 30-32.
55. R. Mehrabian: *International Metals Reviews*, 1982, vol. 27, no. 4, pp. 185-208.
56. E.J. Lavernia, E. Gomez, and N.J. Grant: *Journal of Materials Science and Engineering*, 1987, vol. 95, pp. 225-36.
57. M. Veistinen, E.J. Lavernia, M. Abinante, and N.J. Grant: *Materials Letters*, 1987, vol. 5, no. 10, pp. 373-79.
58. J. Baram, M. Veistinen, E.J. Lavernia, and N.J. Grant: Department of Materials Science and Engineering, Massachusetts Institute of Technology, unpublished research, Cambridge, MA, 1987.
59. J.D. Ayers and I.E. Anderson: *Journal of Metals*, Aug. 1985, vol. 37, no. 8, pp. 16-21.
60. L.J.D. Sully: *American Foundrymen's Society Transactions*, 1976, vol. 84, pp. 735-44.
61. M.C. Flemings: in *Metallurgical Treatises*, J.K. Tien and J.F. Elliott, eds., TMS-AIME, Warrendale, PA, 1981, pp. 291-300.
62. P. Bewley and B. Cantor: in *International Conference on Rapidly Solidified Materials*, P. Lee and R. Carbonara, eds., ASM, Metals Park, OH, 1986, pp. 15-21.
63. A.H. Shapiro: *The Dynamics and Thermodynamics of Compressible Fluid Flow*, Ronald Press Co., NY, 1953, vol. 1, p. 85.
64. J.D. Anderson, Jr.: *Modern Compressible Flow*, ch. 11. McGraw-Hill NY, 1982.
65. J.M. Beer and N.A. Chigier: *Combustion Aerodynamics*, Robert E. Krieger, ed., ch. 6. Malabar, FL, 1983.
66. J. Szekely, J.W. Evans, and H.Y. Sohn: *Gas-Solid Reactions*, Academic Press, NY, 1976, p. 13.
67. G. Forsythe, M.A. Malcolm, and C.B. Moler: *Computer Methods for Mathematical Computations*, ch. 6. Prentice-Hall, Englewood Cliffs, NJ, 1977.
68. W.F. Ames: *Numerical Methods for Partial Differential Equations*, 2nd Ed., ch. 2. Academic Press, NY, 1977.
69. W. Kurz and D.J. Fisher: *Fundamentals of Solidification*, Trans. Tech. Publication, Switzerland, 1984, pp. 65-92.
70. D. Apelian, B.H. Kear, and H.W. Schandler: in *Rapidly Solidified Crystalline Alloys*, S.K. Das, B.H. Kear, and C.M. Adam, eds., TMS-AIME, Warrendale, PA, 1985, pp. 93-109.
71. J. Madejski: *International Journal of Heat and Mass Transfer*, 1976, vol. 19, pp. 1009-13.
72. E.J. Lavernia, E. Gutierrez-Miravete, J. Szekely, and N.J. Grant: *International Journal of Rapid Solidification*, in press.
73. E. Gutierrez-Miravete, E.J. Lavernia, G. Trapaga, and J. Szekely: *International Journal of Rapid Solidification*, in press.
74. E.J. Lavernia: Department of Mechanical Engineering, University of California at Irvine, Irvine, CA, unpublished research, 1988.